

MHD Simulations of Strongly Magnetized HII Region Evolution: Evidence for Ionized Gas Filamentation

By Samuel Crowe, under the mentorship of
Professor Zhi-Yun Li and Dr. Yisheng Tu.
Department of Astronomy, University of Virginia

This thesis is submitted in partial completion of the requirements of the BS Astronomy-Physics major.

MHD Simulations of Strongly Magnetized HII Region Evolution: Evidence for Ionized Gas Filamentation

SAMUEL CROWE,¹ YISHENG TU,¹ AND ZHI-YUN LI¹

¹*Dept. of Astronomy, University of Virginia, Charlottesville, Virginia 22904, USA*

ABSTRACT

Recent JWST observations of HII regions in the Central Molecular Zone have shown a highly filamentary morphology distinct from HII regions in the solar neighborhood. We present magnetohydrodynamic (MHD) simulations, using the **Athena++** simulation framework, of strongly magnetized ($\beta \ll 1$) HII region evolution that effectively recreate the formation of these ionized gas filaments. HII region evolution has been simulated in a 30 pc^3 box, in distinct models with pre-placed overdensities in the ambient medium and overdensities that have been generated with driven turbulence. We find that when these overdensities are seeded in the ambient medium before the birth of the ionizing source, the photoionized plasma stripped off of these dense blobs is funneled into long filaments. Given that these filaments are effectively magnetically-confined flows of photoionized gas, their density and curvature are determined by the density of the blob and the geometry of the configuration.

Keywords: ISM: HII regions, Sgr C

1. INTRODUCTION

HII regions, the regions of hot, ionized gas that are typically associated with star-forming molecular clouds, stand at an important intersection in contemporary astrophysics. In their earliest, compact phases, HII regions provide an indelible contribution to the internal stellar feedback that disperses molecular clouds before the conversion of gas to newborn stars is complete (Zucker-[man & Evans 1974](#); [Krumholz et al. 2007](#)). As signposts of star formation, particularly massive star formation, which itself has an outsized impact on the evolution of galaxies (see [Tan et al. 2014](#); [Rosen et al. 2020](#), for recent reviews), HII regions are crucial diagnostics of star formation rates in the Milky Way and other galaxies ([Kennicutt 1989](#); [Williams & McKee 1997](#); [Lim & De Buizer 2019](#)). Likewise, the containment of ionizing radiation to the HII region of a young OB association (i.e., the escape fraction) governs the interstellar and intergalactic radiation field, the ionization of the interstellar medium, and the observed dispersion measure of pulsars throughout the galaxy, among other important as-

trophysical processes (see [McKee & Williams 1997](#), and references therein).

Only recently, however, has the evolution of HII regions, and their impact on star formation, been considered in more extreme regions. The Central Molecular Zone (CMZ), the central few hundred parsecs of the Milky Way ([Henshaw et al. 2023](#)), is one such region, characterized by molecular cloud densities, temperatures, turbulence, and magnetic field strengths orders of magnitude above those typically observed in the Galactic disk (see, e.g., [Bally et al. 1987, 1988](#); [Giveon et al. 2002](#); [Ferrière 2009](#); [Kruijssen et al. 2014](#); [Ginsburg et al. 2016](#)).

Recent James Webb Space Telescope (JWST) observations of the CMZ massive star-forming region Sagittarius C (Sgr C), at a galactocentric radius (in projection) of $\sim 75 \text{ pc}$, have revealed a striking filamentary morphology in the Sgr C HII region in the Br α hydrogen recombination line ([Crowe et al. 2025](#)). [Bally et al. \(2025\)](#) suggested several possible origins for the observed filaments, including supernova remnants, photo-dissociation regions, and fossil outflow lobes, but presented compelling evidence that a significant population of the filaments are sculpted by magnetic fields, particularly the large-scale poloidal (i.e., perpendicular to the galactic plane) field in the CMZ.

Magnetic fields play an important role in the evolution of star-forming regions (Hennebelle & Inutsuka 2019; Pattle & Fissel 2019; Pattle et al. 2023), and several papers have probed the effects of magnetic fields on HII region evolution in particular. Krumholz et al. (2007) introduced a magneto-hydrodynamic (MHD) code and incorporated it with existing hydrodynamic frameworks for HII region modeling. Arthur et al. (2011) and Zamora-Avilés et al. (2019) found that magnetic fields inhibit HII region expansion perpendicular, but not parallel, to the field lines, producing elongated ellipsoid (rather than spherical) HII regions. Gendelev & Krumholz (2012) extend this treatment to “blister” HII regions, configurations where an ionizing source is positioned between a high- and low-density medium (e.g., at the edge of a dense molecular cloud), finding that the HII region is still elongated along the magnetic field lines, and that the inclusion of magnetic effects may increase the injection rate of energy into the cloud.

Finally, Mackey & Lim (2011) present MHD simulations of “pillars” of neutral gas at HII region edges under uniform B-fields up to $160 \mu\text{G}$ ($\beta \sim 0.01$). When strong B-fields are included perpendicular to the pillar axis, elongated “ribbons” of ionized plasma were observed expanding perpendicular to the pillar axis (parallel to the B-field). Fields parallel to the pillar axis tended to generate “ribbons” of ionized gas extending back into the HII region, parallel to the pillar axis. The authors suggest that in highly magnetized HII regions, such filamentary structures would be readily observable in plasma tracers, such as the Br α line.

Most literature on HII region evolution in a magnetized medium considers relatively weak ($\leq 50 \mu\text{G}$) fields typical of Galactic disk star forming regions (see, e.g., Van Eck et al. 2011). The magnetic fields in the CMZ are orders of magnitude stronger than in the Galactic disk near the Sun, with CMZ field strengths ranging from $100 \mu\text{G}$ to over 1 mG in dense molecular clouds (Ferrière 2009). Therefore, it may be expected that magnetic fields have an outsized effect on the evolution of HII regions in the CMZ, particularly in producing the filamentation observed in Sgr C.

In this paper, we present MHD simulations of highly-magnetized HII region evolution in CMZ-like conditions that attempt to replicate the formation of the ionized gas filaments observed in Sgr C. The paper is organized as follows. The simulation setup is described in §2. The results are shown and discussed in §3 and §4, respectively. A conclusion is made in §5

2. METHODS

We present a suite of radiation magnetohydrodynamic (RMHD) simulations of HII region evolution using the grid-based code **Athena++** (Stone et al. 2020) with additional physics modules for adaptive ray-tracing and photochemistry. The additional radiation modules are largely similar to those used in Kim et al. (2021), which is an augmented version of the setup used in Kim et al. (2017, 2018, 2019).

The evolution of a radiatively and magnetically dominated HII region is governed by the following set of equations:

$$\frac{\partial \rho}{\partial t} + \nabla \cdot (\rho \mathbf{v}) = 0, \quad (1)$$

$$\frac{\partial(\rho \mathbf{v})}{\partial t} + \nabla \cdot [\rho \mathbf{v} \mathbf{v} + P^* \mathbb{I} - \frac{\mathbf{B} \mathbf{B}}{4\pi}] = \mathbf{f}_{\text{rad}}, \quad (2)$$

$$\frac{\partial E}{\partial t} + \nabla \cdot [(E + P^*) \mathbf{v} - \frac{\mathbf{B}(\mathbf{B} \cdot \mathbf{v})}{4\pi}] = \mathcal{G} - \mathcal{L} + \mathbf{v} \cdot \mathbf{f}_{\text{rad}}, \quad (3)$$

$$\frac{\partial \mathbf{B}}{\partial t} - \nabla \times (\mathbf{v} \times \mathbf{B}) = 0, \quad (4)$$

$$\frac{\partial n_s}{\partial t} + \nabla \cdot (n_s \mathbf{v}) = n_H \mathcal{C}_s, \quad (5)$$

$$\frac{\partial \mathbf{I}}{\partial t} + c \mathbf{n} \cdot \nabla \mathbf{I} = \mathbf{S}(\mathbf{I}, \mathbf{n}), \quad (6)$$

where P^* is the total pressure, including the gas thermal pressure and magnetic pressure, and \mathbf{f}_{rad} is the radiative force per unit volume. To represent the heating (\mathcal{G}) and cooling (\mathcal{L}) due to radiation, we adopt a simple temperature prescription, used by Kim et al. (2017, 2018, 2019), where temperature is assigned as a smoothly varying function of the fraction of neutral gas, i.e.

$$T = T_{\text{ion}} - \left(\frac{x_n}{2 - x_n} \right) (T_{\text{ion}} - T_{\text{neu}}) \quad (7)$$

where $x_n = n_{\text{H}^0}/n_{\text{H}}$ is the neutral gas fraction and $T_{\text{ion}} = 8000 \text{ K}$ and $T_{\text{neu}} = 20 \text{ K}$ are the temperatures of the fully ionized and fully neutral gas, respectively. The gas thermal pressure and energy are subsequently calculated through the adiabatic equation of state. Since most dynamics occur in the fully ionized region, we assume the gas is in the ideal MHD limit (Eq. 4) throughout the simulation. We ignore the effects of gravity as gravity is not expected to be important in the magnetically and radiatively dominated environment we model. The remaining symbols have their usual meanings.

Photo-ionization is treated by solving the radiation transfer equation (Eq. 6) with photon sources representing the ionizing photons emitted by hot stars (such

as O stars and B stars) in CMZ. The hydrogen ionization fraction due to radiation is calculated with Eq. 5 using a simplified photochemistry network including photoionization and recombination. Because of the high ionizing photon emission rates of the hot stars modeled in the simulation, most gas in the simulation stays either fully ionized (if inside the ionization front) or fully neutral (if outside the radiation front).

A suite of RMHD simulations were conducted with a suite of parameters selected to roughly correspond to the conditions in Sgr C (see Bally et al. 2025). We model a 30 pc^3 region with 256 cells in each direction (i.e., the resolution is 0.12 pc per cell). An ionizing source was placed at $(x, y, z) = (0, 0, 0)$ with an ionizing photon emission rate of $Q_0 = 1 \times 10^{50} \text{ s}^{-1}$. To model the magnetically-dominated environment in Sgr C, a \hat{z} -direction magnetic field of 1 mG was added so that the maximum plasma- β is < 1 in all regions (average $\beta \approx 10^{-5}$). The outflow boundary condition is applied at all simulation boundaries.

With the above setup, we present two models: We first illustrate one possible filament-forming mechanism using a model with artificially placed spherical overdensities in the ambient medium (hereafter referred to as “blobs”). Two blobs, each 1 pc in radius, are placed at $(x, y, z) = (5, 0, 0)$ and $(x, y, z) = (-5, 0, 5)$. The density in the blobs is uniform at 1000 H/cm^{-3} . The remaining simulation volume is filled with an ambient medium of density 100 H/cm^{-3} .

In the second model, we demonstrate how the mechanism identified in the first model naturally forms filament-like structures in a more realistic environment where density inhomogeneities were seeded by turbulence rather than artificially placing blobs. To naturally generate a density inhomogeneity, we drive turbulence in the model for 20 Myrs . The turbulence driving time is chosen such that the resulting density contrast reflects conditions typical of molecular clouds (Rathborne et al. 2014). We then stop the turbulence and introduce the magnetic field and ionization source. The turbulence is driven with an energy spectrum

$$E(k) \propto k^{-2} \quad (8)$$

where $k = 2\pi/\lambda$ is the wavenumber for a given eddy with wavelength λ . Energy was injected into the system at a rate of $2.23 \times 10^{34} \text{ erg s}^{-1}$, with wave numbers between 2 and 128. An initial ambient density of 600 H/cm^{-3} is used to mitigate the mass loss at the simulation boundary during the turbulence driving phase. The average density of the ambient medium upon activation of the ionizing source was much lower, close to the 100 H/cm^{-3} used for the blob simulations.

3. RESULTS

3.1. Simulation with pre-placed blobs

Figure 1 shows various quantities of the simulation, along the $x - z$ plane, in the first model, with pre-set blobs. The first three panels, (a), (b), and (c), show cuts along the $y = 0$ plane, where the blobs are placed, of the number density, $n(\text{H})$, at three different times. At 0.3 Myr (b), two effects are noticeable in the blob at $z = 0$. Firstly, the blob has begun to be compressed along the $z = 0$ plane; by 1.3 Myr (c), the blob has been flattened out into a one-dimensional stream of gas along $z = 0$. Inspecting panel (d), which shows the column density of ionized gas along the line-of-sight, it becomes obvious that this stream is made up almost entirely of neutral gas (i.e., there is little to no ionized gas along the stream). Much of this stream is likely made up of neutral gas from the ambient medium, rather from the blob, that is shielded from ionizing radiation by the blob. Secondly, by 0.3 Myr , a bright, filamentary stream of dense ionized gas has formed at the tip of the blob, at $x \approx 4 \text{ pc}$, about 10 pc in length. By 1.3 Myr , this filament of ionized gas has almost expanded to the length of the simulation domain ($\approx 25 \text{ pc}$ long, see panels [c] and [d]).

Panel (e) shows the z -velocity, v_z , with arrows showing the velocity vectors. A velocity enhancement is apparent at $x \approx 4 \text{ pc}$, the location of the filament: above $z = 0$, the velocity is large and positive (around 20 km s^{-1}) and below $z = 0$, the velocity is large and negative (around -20 km s^{-1}). This implies that the filamentary structure is in fact a *flow* of ionized gas, rather than a static accumulation; in fact, the flow is supersonic, with mach numbers ranging from $1.5 \sim 3$ along the length of the filament. The lower right panel shows the plasma β parameter, i.e.

$$\beta = P_T/P_B \quad (9)$$

where P_T and P_B are the thermal and magnetic pressures, respectively. $\beta < 1$ across the entire simulation domain, implying that all of the ionized plasma is magnetically dominated. Within the ionized gas filament, β is enhanced, ranging from a few hundredths at the “tip” of the filament to ~ 0.005 across the rest of its extent.

These last two observations, the low plasma β of the filament and its high velocity, outflowing from the tip of the neutral gas blob, implies that the filament is a *magnetically confined plasma flow*, i.e. a flow of ionized gas that has been stripped off (photoablated) from the surface of the dense neutral gas blob and forced to flow in line with the magnetic field in the \hat{z} -direction. The enhancement of β , and therefore the thermal pressure, at the tip of the blob (panel [f]), is also noteworthy, implying a negative pressure gradient out to increasing

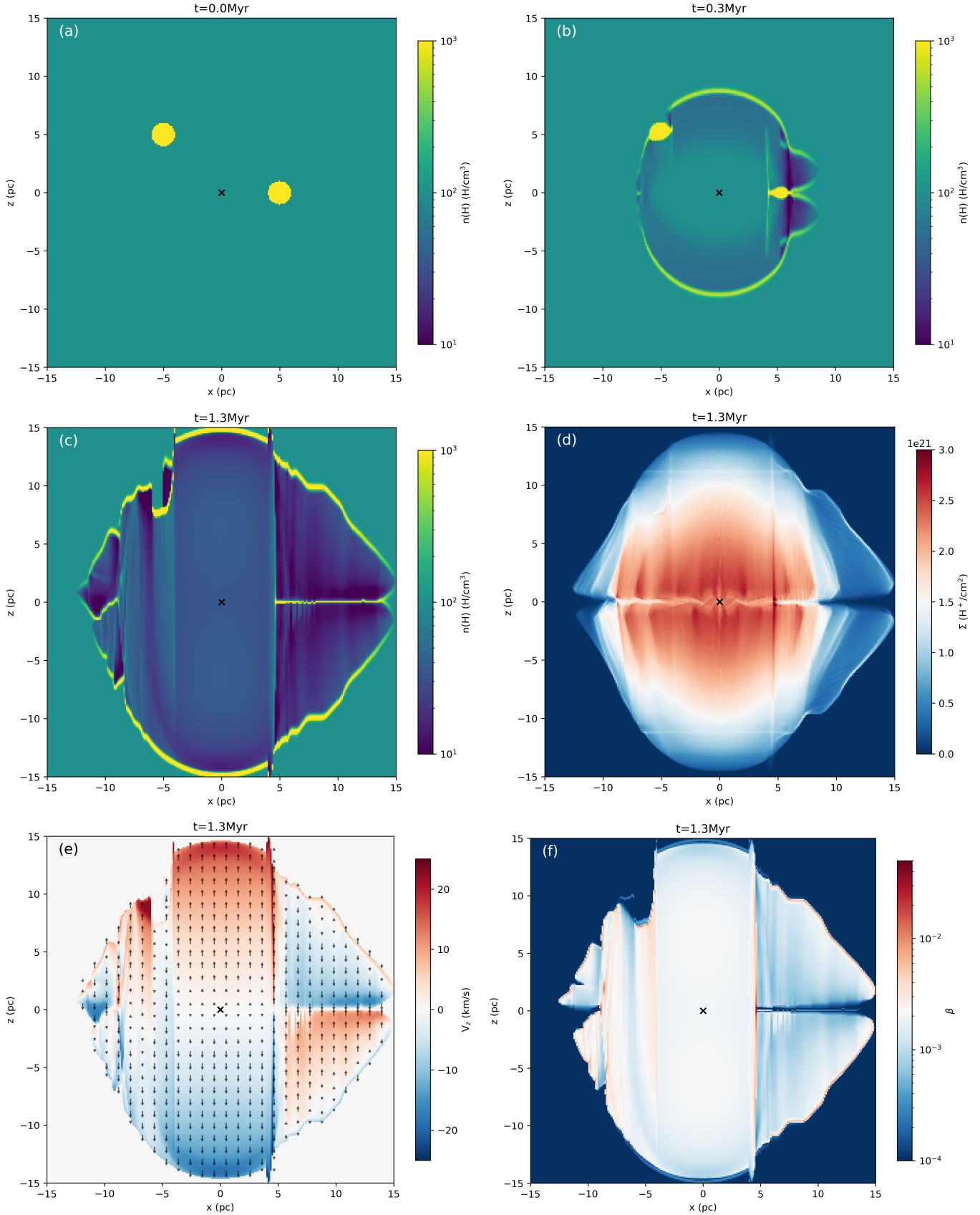


Figure 1. Select cutaways from the simulation run with preset blobs. Panel (a) shows an $x-z$ slice (along $y=0$) of the number density at $t=0$, i.e. the initial condition before activation of the ionizing source. Panels (b) and (c) show the same at $t=0.3$ and $t=1.3$ Myr, respectively. Panel (d) shows the integrated *ionized* gas density along the line of sight, i.e. the column density. Panel (e) shows the z -velocity, v_z , along an $x-z$ slice ($y=0$) with velocity vectors shown in black and scaled to the magnitude of the velocity. Panel (f) shows an $x-z$ slice (along $y=0$) of the plasma β , i.e. thermal pressure divided by magnetic pressure. The location of the ionizing source is marked with a black cross in all panels.

values of $|z|$ that causes the filament to “spread” out to the full extent seen by 1.3 Myr.

Interestingly, the left blob in the simulation, which is identical to the right blob except for its placement at $(x, y, z) = (-5, 0, 5)$, displays a markedly different morphology, particularly at later times. At $t = 0.3$ Myr (panel [b]), a slight density enhancement can be seen on the right side of the blob as it is being photoionized, but by 1.3 Myr (panels [c], [d]), it becomes clear that the flow of plasma from this blob resembles a thick, two-dimensional “sheet” (or three-dimensional “cylinder”) rather than a one-dimensional “filament”. This is due to the fact that the entire bottom face of the blob is exposed to the ionizing source, meaning that the flow of ionized gas is much more extended along the x -direction than the flow of plasma from the blob at $z = 0$. The slight enhancement of thermal pressure at the tip of the blob (panel [f]) suggests that this flow of ionized plasma is indeed caused by photoionization of the outer layer of the blob, similar to the blob at $z = 0$. Clearly, the formation of a filament, in this simulation setup, depends closely on the geometry of the configuration. The $z = 0$ blob is confined and compressed by the photo-evaporative flows from above and below the midplane, and the resulting filament formation is enhanced by the mirror symmetry along the z -axis, which may not be present in real clouds. The lack of symmetry caused the off-middle-plane blob to be pushed away together with the ambient medium, forming a corrugated surface that facilitated the formation of a “sheet” rather than a “filament”.

3.2. Simulation with driven turbulence

Figure 2 shows two panels, along the $x - z$ plane, in the second simulation run, at the time the ionizing source is activated (denoted as $t_0 = 20$ Myr). The left panel shows the total number density, $n(\text{H})$, in the $y = 0$ plane, and the right panel shows the column density of gas along the line-of-sight. As the ionizing source has just been activated, all gas is neutral at this stage. Note the large fluctuations (from < 10 to a few $\times 10^3$ H/cm^3) in the ambient medium compared to the first simulation setup, which assumed a completely uniform initial density; this creates pockets of low- and high-density that emulate the pre-set “blobs” considered previously, but in a more organic environment.

Figure 3 shows several panels, along the $x - z$ plane, of the density of ionized and neutral gas at two different times after activation of the ionizing source: 0.5 Myr and 2 Myr. Panels (a) and (b) show the *total* number density of gas (i.e., neutral plus ionized) along the $y = 0$ plane, whereas panels (c) and (d) show the number density of

ionized gas along the $y = 0$ plane. Panels (e) and (f) show the integrated column density of ionized gas (as opposed to total gas in Fig. 2) along the line-of-sight.

At $t - t_0 = 0.5$ Myr, ionized gas filamentation is apparent in two distinct configurations (see panel [c]). Along $x \approx 2.5$ pc, a dense filament extends along the z -axis, originating from the tip of a dense “pillar” of neutral gas that extends into the HII region. This ionized gas filament seems to have been generated by a similar mechanism as the filament shown in Fig. 1 and discussed in §3.1, with the dense “pillar” playing a nearly identical role as the dense blob in the first simulation. This filament is also apparent in the ionized gas column density (panel [e]) and shows the same velocity signature as shown in Fig. 1 panel (e), but with mach numbers closer to ≈ 1 across the filament.

Other, lower density filaments are apparent as well, including the filament (or pair of filaments) at $x \approx -4$ and $x \approx 2$ pc. These filaments do not have an obvious pillar or blob to feed them, but rather are generated by specific geometries in which a “wall” of dense neutral gas at constant x is photoionized (e.g., the wall extending from $x \approx -4$, $z \approx 3 \sim 6$ pc, and from $x \approx 2$, $z \approx 4 \sim 5$ pc in panel [c]), causing an overdensity of magnetically-confined plasma to flow along a filament at constant x . Despite the difference in configuration between these two types of filaments, in underlying mechanism they are essentially identical, as magnetically-confined plasma flows.

At $t - t_0 = 2$ Myr (panels [b], [d], [f]), the HII region has evolved and expanded to the extent that several more pillars (and filaments) are apparent, including those at $(x, z) \approx (-5, -2)$, $(x, z) \approx (-6, 3)$, $(x, z) \approx (6, 7)$, $(x, z) \approx (10, -2)$, $(x, z) \approx (11, 1)$, etc. The ionized gas column density, panel (f), shows a highly filamentary morphology, including filaments around the pillars mentioned above.

Many of the filaments at this time step have a curved appearance, rather than being almost perfectly linear like the filament in Fig. 1. This can be interpreted as the result of rapid photoionization of the pillars; since essentially all of the plasma seeding a given filament comes from the tip of the pillar, as the tip moves (the pillar is ionized), the filament (the flow of ionized gas) shifts as well. For a specific treatment and explanation of this phenomenon, see Appendix A.

4. DISCUSSION

4.1. Comparison with Sgr C

As was established in §1, this study was motivated by JWST observations of ionized gas filamentation in the Sgr C star-forming region, in the Central Molecular

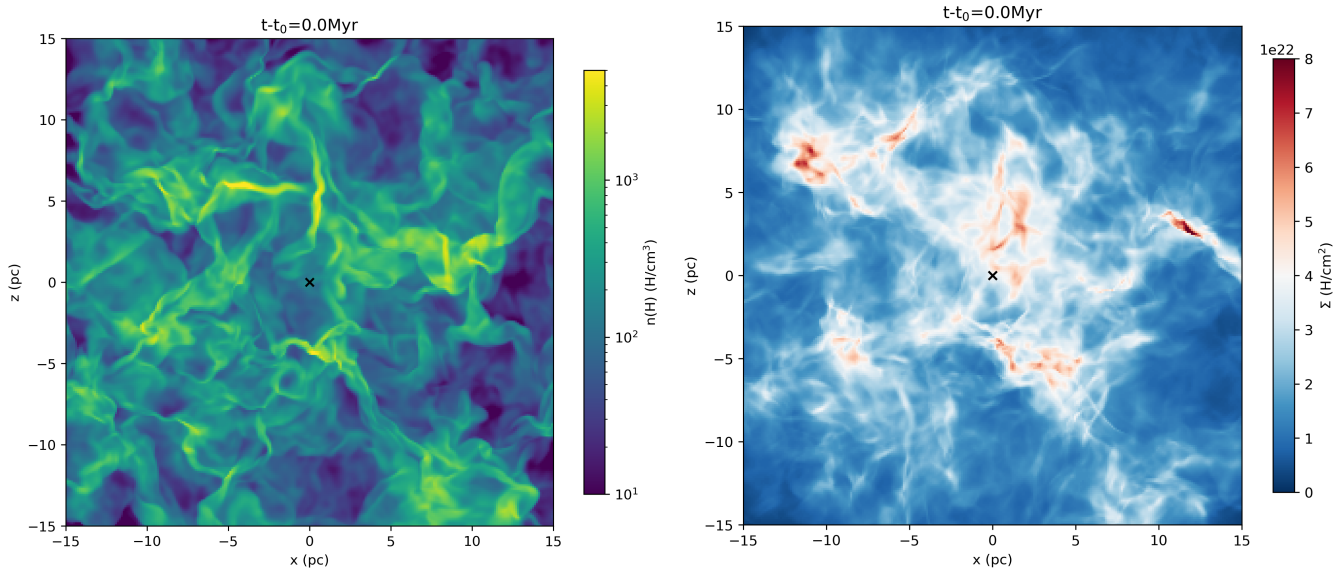


Figure 2. Gas density along the $x - z$ plane at the time of activation of the ionizing source (t_0) in the simulation run with driven turbulence. The left panel shows a slice of the gas density in the $y = 0$ plane, and the right panel shows the integrated gas density along the line-of-sight. The ionizing source is marked with a black cross in both panels.

Zone, which are detailed by Bally et al. (2025). As such, an in-depth comparison with the results presented in §3 is warranted. We choose to concern ourselves with the second simulation run, which includes a period of driven turbulence, as we view this simulation as closer to a real environment.

One of the most direct possible comparisons is the density of the filaments observed in our simulation versus that reported in Bally et al. (2025). We select as a representative the filament located along $x \approx 2.5$ shown in the panel (c) of Fig. 3, at a time $t - t_0$ of 0.5 Myr. The column density of this filament was measured using the column density map shown in panel (e) of Fig. 3 to be around $3.91 \times 10^{21} \text{ H}^+/\text{cm}^2$, which compares to $3.46 \times 10^{21} \text{ H}^+/\text{cm}^2$ just off the filament, or a “background-subtracted” column density of $4.5 \times 10^{20} \text{ H}^+/\text{cm}^2$ for the filament alone. A depth of this feature of $\approx 0.35 \text{ pc}$ was measured from a $y - z$ density slice along the filament axis. Dividing the filament’s column density by its depth yields a filament density of around $400 \text{ H}^+/\text{cm}^3$, a factor of 4 higher than the mean ionized gas density within the HII region, which is $\approx 100 \text{ H}^+/\text{cm}^3$.

This measured density is markedly different from the density of the filaments measured by Bally et al. (2025), who, for a slightly larger average HII region density of $\sim 200 \text{ H}^+/\text{cm}^3$, reported filament densities ranging from a few $\times 10^3$ to $1 \times 10^4 \text{ H}^+/\text{cm}^3$. This difference may be due to more complicated line-of-sight effects in Sgr C, or further confinement of the plasma in Sgr C due to additional unmodeled physical processes; it is worth

noting that unlike the simulated filaments, which extend for several or dozens of parsecs, the filaments in Sgr C have a maximum length of $\approx 1 \text{ pc}$. It is possible that, for example, if the Sgr C HII region were a region of relatively low density embedded within a higher-density environment (potentially due to, e.g., the clearing of local material due to stellar feedback), the confinement of the filaments in such a smaller space could cause their density to be higher than measured in our model, which assumes a completely uniform medium. It is also worth noting that the line-of-sight depth is poorly constrained in Sgr C, unlike in our simulation, meaning that the reported number densities in Sgr C represent upper limits on the density (Bally et al. 2025).

The comparison between the shape, extent, and age of the simulated HII region and Sgr C is also worth exploring. The “core” of the brightest emission in the Sgr C HII region measures around 7 pc on its long dimension (roughly parallel to the galactic plane) and around 5 pc on its short dimension (perpendicular to the galactic plane). The “core” of the most dense portion of the simulated HII region is around 10 pc in all dimensions, or about twice as large as Sgr C, although there is some slight preferential elongation along the x - and y -axes at later times (see panels [d], [f] of Fig. 3). The $\approx 2\times$ difference in overall size is likely attributable to the $\approx 2\times$ difference in average density between Sgr C and the simulated medium. The slightly lower density for the simulation runs was chosen as a practical consideration, as a more dense, compact HII region would be more computationally intensive to model (particularly

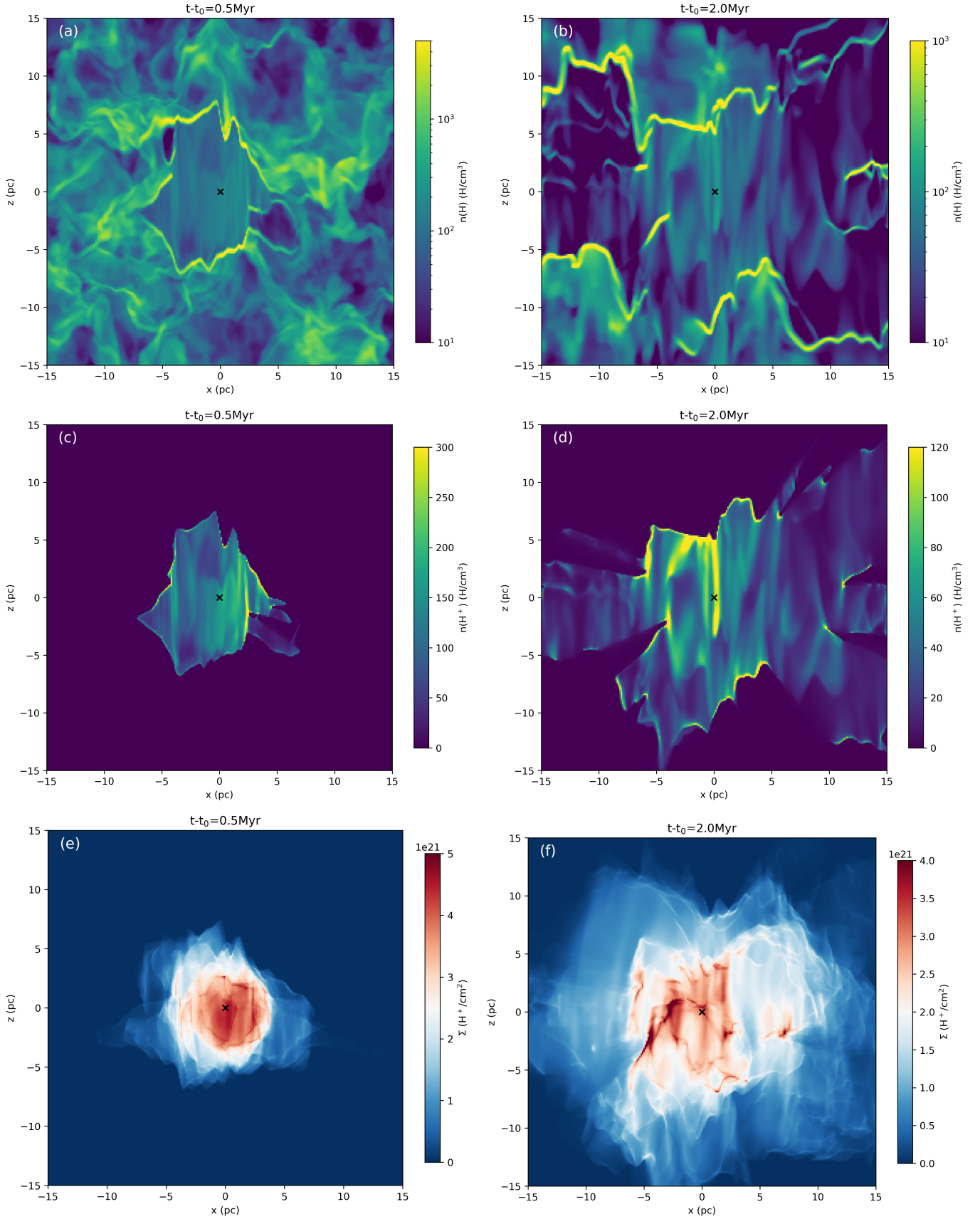


Figure 3. Select cutaways from the simulation run with driven turbulence. Panels (a) and (b) show $x-z$ slices (along $y=0$) of the *total* number density of gas at $t-t_0=0.5$ and 2 Myr, respectively. Panels (c) and (d) show the same but for the *ionized* gas number density. Panels (e) and (f) show the integrated *ionized* gas density along the line of sight, i.e. the column density. The location of the ionizing source is marked with a black cross in all panels.

in the demands on increased resolution) compared to a diffuse, extended one. Future simulations may be able to more accurately model in high-resolution an environment with a Sgr C-like density.

There are some striking similarities in the shape of the two HII regions. As mentioned, both the simulated and observed HII regions are nearly spherical (circular in the case of Sgr C), but slightly elongated *perpendicular* to the magnetic field lines (if, in the case of Sgr C, the poloidal component of the CMZ magnetic field is the dominant one, which is implied by the statistical preference of filament orientations along the poloidal component of the field; see Fig. 6 of Bally et al. 2025). This result is quite unexpected given the suggestion of several previous studies that magnetized HII regions are distorted and elongated *parallel* the field lines (Krumholz et al. 2007; Arthur et al. 2011; Zamora-Avilés et al. 2019; Gendelev & Krumholz 2012). It is possible that this phenomenon, the elongation of the HII region perpendicular to the field, could be due to the lifting of material away from the midplane by the strong perpendicular magnetic field, allowing the ionizing radiation to cleave through regions of higher density more easily and carve out a lower-density “tunnel” along the midplane (see panels [b], [d] of Fig. 3). However, this is only one possible mechanism.

Another interesting feature is the presence of a diffuse, filamentary “halo” of ionized gas around the “core” of the HII region, which is seen in both Sgr C and the simulation. This is best seen in panel (f) of Fig. 3 and the top panel of Fig. 4 of (Bally et al. 2025). This diffuse halo implies significant leakage of ionizing photons into the extended medium surrounding each HII region; in the case of the simulation with driven turbulence, this is likely due to the ease with which the ionization front eats through regions of low density, forming the pockets of ionized gas best seen in panel (d) of Fig. 3.

Finally, one interesting comparison between the Sgr C and the simulation presented is the morphology of the filaments themselves. The filaments in Sgr C are generally brighter, shorter, more numerous, and have a wider diversity of curvature and orientation than the filaments in the simulated HII region. The differences in brightness (density), length, and number have been addressed above. The differences in curvature and orientation are more intriguing. Differences in curvature are likely due to lower density in the blob/pillar/wall that feeds the filament, causing the plasma flow to shift as the reservoir of neutral gas is rapidly eroded away; this is explored further in Appendix A. Differences in orientation are harder to treat, as they imply complicated line-of-sight effects in Sgr C that are extremely difficult to model

with the constraints on resolution and magnetic field orientation in the simulation setup used in this work. Particularly, the filamentation in Sgr C often displays a pattern of overlapping or nearly-overlapping filaments with different orientations, e.g. in a cross-hatching pattern (see Fig. 5 and Appendix A of Bally et al. 2025). This implies rapidly varying local magnetic fields, both across the plane of the sky and along the line-of-sight, that are not modeled in the models presented in this paper. Ultimately, more high-resolution simulations with more sophisticated treatment of local magnetic effects will be necessary to approach the precise morphology of the filamentation observed in Sgr C. Further high-resolution observations of the magnetic field orientation in Sgr C with, e.g., ALMA, will also help shed light on the tangled magnetic field structure in the region.

5. CONCLUSIONS

In this paper, we have presented a suite of RMHD simulations of HII region expansion and evolution that effectively demonstrates the formation of ionized gas filaments, similar to those observed by Bally et al. (2025), in strong magnetic fields. We find that these filaments can be explained effectively as magnetically-confined ($\beta \ll 1$) flows of photoionized plasma. These flows must be seeded by a reservoir of dense neutral gas; we present two possible geometries, one in which the reservoir is a freestanding dense “pillar” or “blob”, and one in which the reservoir is a long “wall” of neutral gas parallel to the magnetic field. In both cases, the curvature of the filament is dependent on the density of the reservoir.

Although we are able to replicate the formation of both curved and straight ionized gas filaments, we note several discrepancies between our models and Sgr C. First, the filaments in our models are longer and less dense than the filaments in Sgr C, which is potentially due both to constraints on the simulation parameters and the environment around Sgr C. Second, we are not able to replicate the diversity of filament orientations observed in Sgr C, and the complicated structure along the line-of-sight. We expect that this will be more difficult to treat, involving greater knowledge of the local magnetic field in Sgr C and more sophisticated, higher-resolution simulations accounting for rapid variations in the local magnetic field.

Acknowledgments: This work is based on simulations run using computing resources from UVA research computing (RIVANNA). S.T.C. acknowledges support from the award JWST-GO-04147.003-A.

REFERENCES

- Arthur, S. J., Henney, W. J., Mellema, G., de Colle, F., & Vázquez-Semadeni, E. 2011, *MNRAS*, 414, 1747, doi: [10.1111/j.1365-2966.2011.18507.x](https://doi.org/10.1111/j.1365-2966.2011.18507.x)
- Bally, J., Stark, A. A., Wilson, R. W., & Henkel, C. 1987, *ApJS*, 65, 13, doi: [10.1086/191217](https://doi.org/10.1086/191217)
- . 1988, *ApJ*, 324, 223, doi: [10.1086/165891](https://doi.org/10.1086/165891)
- Bally, J., Crowe, S., Fedriani, R., et al. 2025, *ApJ*, 983, 20, doi: [10.3847/1538-4357/ad9d0b](https://doi.org/10.3847/1538-4357/ad9d0b)
- Crowe, S., Fedriani, R., Tan, J. C., et al. 2025, *ApJ*, 983, 19, doi: [10.3847/1538-4357/ad8889](https://doi.org/10.3847/1538-4357/ad8889)
- Ferrière, K. 2009, *A&A*, 505, 1183, doi: [10.1051/0004-6361/200912617](https://doi.org/10.1051/0004-6361/200912617)
- Gendele, L., & Krumholz, M. R. 2012, *ApJ*, 745, 158, doi: [10.1088/0004-637X/745/2/158](https://doi.org/10.1088/0004-637X/745/2/158)
- Ginsburg, A., Henkel, C., Ao, Y., et al. 2016, *A&A*, 586, A50, doi: [10.1051/0004-6361/201526100](https://doi.org/10.1051/0004-6361/201526100)
- Giveon, U., Sternberg, A., Lutz, D., Feuchtgruber, H., & Pauldrach, A. W. A. 2002, *ApJ*, 566, 880, doi: [10.1086/338125](https://doi.org/10.1086/338125)
- Hennebelle, P., & Inutsuka, S.-i. 2019, *Frontiers in Astronomy and Space Sciences*, 6, 5, doi: [10.3389/fspas.2019.00005](https://doi.org/10.3389/fspas.2019.00005)
- Henshaw, J. D., Barnes, A. T., Battersby, C., et al. 2023, in *Astronomical Society of the Pacific Conference Series*, Vol. 534, *Protostars and Planets VII*, ed. S. Inutsuka, Y. Aikawa, T. Muto, K. Tomida, & M. Tamura, 83, doi: [10.48550/arXiv.2203.11223](https://doi.org/10.48550/arXiv.2203.11223)
- Kennicutt, Jr., R. C. 1989, *ApJ*, 344, 685, doi: [10.1086/167834](https://doi.org/10.1086/167834)
- Kim, J.-G., Kim, W.-T., & Ostriker, E. C. 2018, *ApJ*, 859, 68, doi: [10.3847/1538-4357/aabe27](https://doi.org/10.3847/1538-4357/aabe27)
- . 2019, *ApJ*, 883, 102, doi: [10.3847/1538-4357/ab3d3d](https://doi.org/10.3847/1538-4357/ab3d3d)
- Kim, J.-G., Kim, W.-T., Ostriker, E. C., & Skinner, M. A. 2017, *ApJ*, 851, 93, doi: [10.3847/1538-4357/aa9b80](https://doi.org/10.3847/1538-4357/aa9b80)
- Kim, J.-G., Ostriker, E. C., & Filippova, N. 2021, *ApJ*, 911, 128, doi: [10.3847/1538-4357/abe934](https://doi.org/10.3847/1538-4357/abe934)
- Kruijssen, J. M. D., Longmore, S. N., Elmegreen, B. G., et al. 2014, *MNRAS*, 440, 3370, doi: [10.1093/mnras/stu494](https://doi.org/10.1093/mnras/stu494)
- Krumholz, M. R., Stone, J. M., & Gardiner, T. A. 2007, *ApJ*, 671, 518, doi: [10.1086/522665](https://doi.org/10.1086/522665)
- Lim, W., & De Buizer, J. M. 2019, *ApJ*, 873, 51, doi: [10.3847/1538-4357/ab0288](https://doi.org/10.3847/1538-4357/ab0288)
- Mackey, J., & Lim, A. J. 2011, *MNRAS*, 412, 2079, doi: [10.1111/j.1365-2966.2010.18043.x](https://doi.org/10.1111/j.1365-2966.2010.18043.x)
- McKee, C. F., & Williams, J. P. 1997, *ApJ*, 476, 144, doi: [10.1086/303587](https://doi.org/10.1086/303587)
- Pattle, K., & Fissel, L. 2019, *Frontiers in Astronomy and Space Sciences*, 6, 15, doi: [10.3389/fspas.2019.00015](https://doi.org/10.3389/fspas.2019.00015)
- Pattle, K., Fissel, L., Tahani, M., Liu, T., & Ntormousi, E. 2023, in *Astronomical Society of the Pacific Conference Series*, Vol. 534, *Protostars and Planets VII*, ed. S. Inutsuka, Y. Aikawa, T. Muto, K. Tomida, & M. Tamura, 193, doi: [10.48550/arXiv.2203.11179](https://doi.org/10.48550/arXiv.2203.11179)
- Rathborne, J. M., Longmore, S. N., Jackson, J. M., et al. 2014, *ApJL*, 795, L25, doi: [10.1088/2041-8205/795/2/L25](https://doi.org/10.1088/2041-8205/795/2/L25)
- Rosen, A. L., Offner, S. S. R., Sadavoy, S. I., et al. 2020, *SSRv*, 216, 62, doi: [10.1007/s11214-020-00688-5](https://doi.org/10.1007/s11214-020-00688-5)
- Stone, J. M., Tomida, K., White, C. J., & Felker, K. G. 2020, *ApJS*, 249, 4, doi: [10.3847/1538-4365/ab929b](https://doi.org/10.3847/1538-4365/ab929b)
- Tan, J. C., Beltrán, M. T., Caselli, P., et al. 2014, in *Protostars and Planets VI*, ed. H. Beuther, R. S. Klessen, C. P. Dullemond, & T. Henning, 149–172, doi: [10.2458/azu_uapress_9780816531240-ch007](https://doi.org/10.2458/azu_uapress_9780816531240-ch007)
- Van Eck, C. L., Brown, J. C., Stil, J. M., et al. 2011, *ApJ*, 728, 97, doi: [10.1088/0004-637X/728/2/97](https://doi.org/10.1088/0004-637X/728/2/97)
- Williams, J. P., & McKee, C. F. 1997, *ApJ*, 476, 166, doi: [10.1086/303588](https://doi.org/10.1086/303588)
- Zamora-Avilés, M., Vázquez-Semadeni, E., González, R. F., et al. 2019, *MNRAS*, 487, 2200, doi: [10.1093/mnras/stz1235](https://doi.org/10.1093/mnras/stz1235)
- Zuckerman, B., & Evans, II, N. J. 1974, *ApJL*, 192, L149, doi: [10.1086/181613](https://doi.org/10.1086/181613)

APPENDIX

A. MODEL WITH LOWER BLOB DENSITIES: CURVED FILAMENTS

In order to demonstrate the mechanism by which a *curved* ionized gas filament, discussed in §3.2, could form, we present a model with identical setup to the pre-set blob simulation described in §2, but with blob densities of 250 H/cm^{-3} rather than 1000 H/cm^{-3} , i.e. $4\times$ lower, only $2.5\times$ more dense than the ambient medium.

The results are presented in Figure 4 (similar to Fig. 1). Panel (a) shows the number density, $n(\text{H})$, on an $x-z$ slice along $y=0$, at $t=0$, i.e. the initial condition. Panel (b) shows the same at $t=1.3 \text{ Myr}$. It can be seen that, in contrast to the filament in panel (b) of Fig. 1, this filament (density enhancement) displays a curved morphology, which is reinforced by the integrated ionized gas column density shown in panel (c) and velocity plot shown in panel (d). This effect can be explained by the lower density of the neutral gas reservoir, which leads to a more rapid depletion of neutral gas as the ionization proceeds. Because the filament (ionized gas flow) is sourced at the “tip” of the neutral gas reservoir, the rapid erosion of the “tip” means that as ionization proceeds, separate, connected channels of ionized gas, at different x -values, are created, giving the appearance of a curved filament.

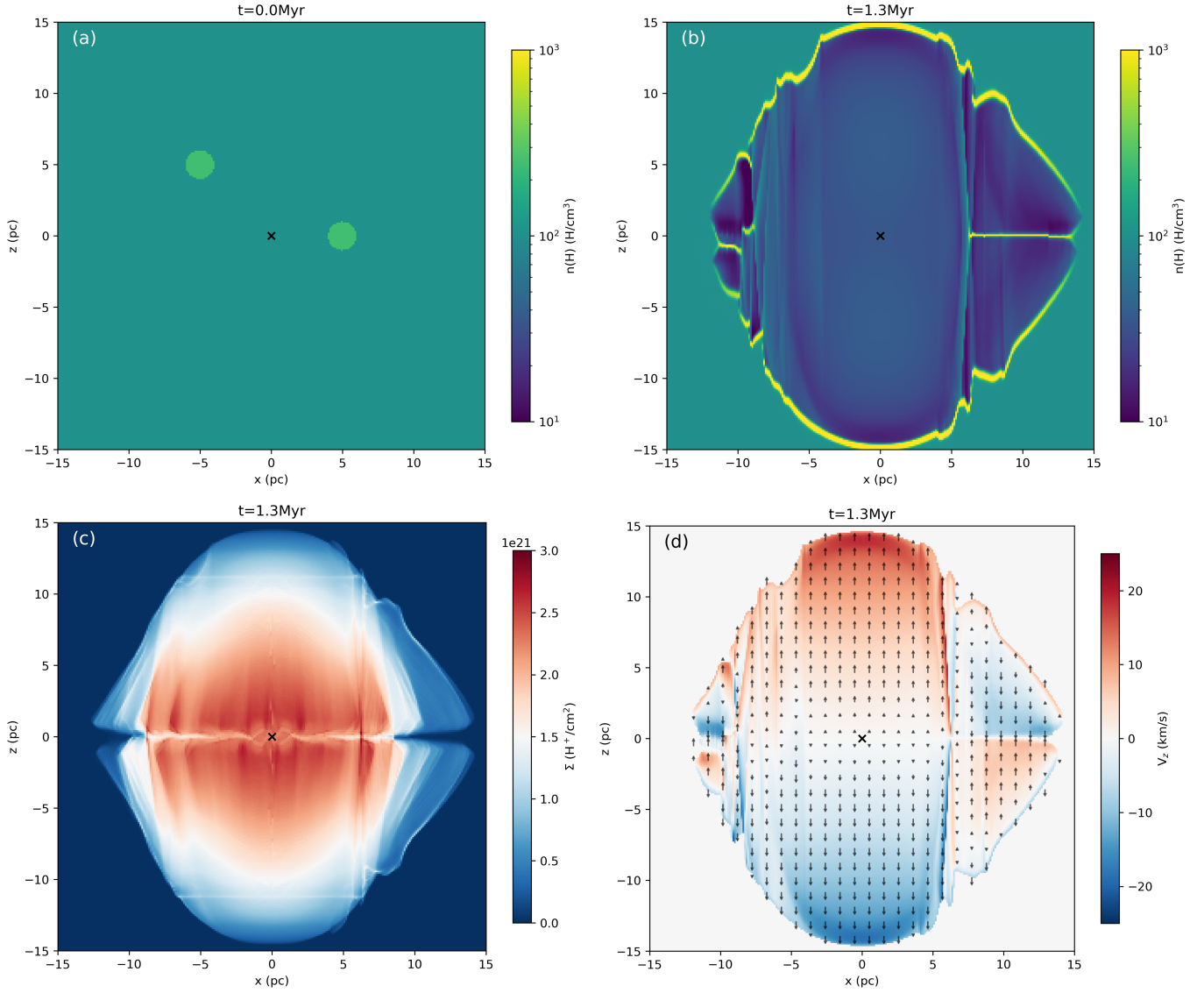


Figure 4. Cutaways from a simulation run with preset blobs of lower density than presented in §3.1 and Fig. 1. Panel (a) shows an $x - z$ slice (along $y = 0$) of the number density at $t = 0$, i.e. the initial condition before activation of the ionizing source. Panel (b) shows the same at $t=1.3$ Myr. Panel (c) shows the integrated ionized gas density along the line of sight, i.e. the column density. Panel (d) shows the the z -velocity, v_z , along an $x - z$ slice ($y = 0$) with velocity vectors shown in black and scaled to the magnitude of the velocity. The location of the ionizing source is marked with a black cross in all panels.